

# Low Overhead Online Data Flow Tracking for Intermittently Powered Non-volatile FPGAs

XINYI ZHANG, University of Pittsburgh  
CLAY PATTERSON, Oklahoma State University  
YONGPAN LIU, Tsinghua University  
CHENGMO YANG, University of Delaware  
CHUN JASON XUE, City University of Hong Kong  
JINGTONG HU, University of Pittsburgh

---

Energy harvesting is an attractive way to power future IoT devices since it can eliminate the need for battery or power cables. However, harvested energy is intrinsically unstable. While FPGAs have been widely adopted in various embedded systems, it is hard to survive unstable power since all the memory components in FPGA are based on volatile SRAMs. The emerging non-volatile memory based FPGAs provide promising potentials to keep configuration data on the chip during power outages. Few works have considered implementing efficient runtime intermediate data checkpoint on non-volatile FPGAs. To realize accumulative computation under intermittent power on FPGA, this paper proposes a low-cost design framework, Data-Flow-Tracking FPGA (DFT-FPGA), which utilizes binary counters to track intermediate data flow. Instead of keeping all on-chip intermediate data, DFT-FPGA only targets on necessary data that is labeled by off-line analysis and identified by an online tracking system. The evaluation shows that compared with state-of-the-art techniques, DFT-FPGA can realize accumulative computing with less off-line workload and significantly reduce online roll-back time and resource utilization.

*This paper has been accepted by ACM Journal on Emerging Technologies in Computing Systems (JETC).*

CCS Concepts: •**Computer systems organization** → **Embedded systems**; *Redundancy*; Robotics; •**Networks** → Network reliability;

Additional Key Words and Phrases: energy harvesting, non-volatile FPGA, checkpoint, high-level-synthesis, data flow

## ACM Reference format:

Xinyi Zhang, Clay Patterson, Yongpan Liu, Chengmo Yang, Chun Jason Xue, and Jingtong Hu. 2019. Low Overhead Online Data Flow Tracking for Intermittently Powered Non-volatile FPGAs. *ACM Trans. Graph.* 0, 0, Article 0 (2019), 19 pages.

DOI: 00.0000/0000000.0000000

---

## 1 INTRODUCTION

FPGAs have been widely adopted in various embedded systems that are powered by batteries. However, in the emerging Internet of Things (IoT)[1–3], which is full of tiny, cost-sensitive, and space constrained widgets, batteries are no longer an ideal power supply due to poor scalability, recharging and safety concerns. Out of all possible alternatives, energy

---

Permission to make digital or hard copies of all or part of this work for personal or classroom use is granted without fee provided that copies are not made or distributed for profit or commercial advantage and that copies bear this notice and the full citation on the first page. Copyrights for components of this work owned by others than ACM must be honored. Abstracting with credit is permitted. To copy otherwise, or republish, to post on servers or to redistribute to lists, requires prior specific permission and/or a fee. Request permissions from [permissions@acm.org](mailto:permissions@acm.org).

© 2019 ACM. Manuscript submitted to ACM

harvesting systems are becoming one of the most promising candidates because they convert ambient energy from their surroundings. Some of the widely known energy harvesting techniques include Photovoltaics (PV), Thermoelectric generators (TEGs), and Piezoelectric (PZ). A device equipped with these harvesters can utilize the converted energy directly or recharge its energy storage (e.g. capacitors). The ease of access to power makes it a very competitive power source for portable devices. However, there are two primary challenges for such energy harvesting systems: unstable power and low power input.

Even though there are ultra-low power FPGAs such as the Lattice iCE40 series, which can work in  $\mu W$  [4], the unpredictability of available energy renders the power intermittent which will interrupt computations. The intermittent power will interrupt computations. In such a condition, long computations may be prohibited since the intermediate data will be lost and the computation has to start over from the beginning. Thus, it is essential to preserve the FPGA *configuration data* and *intermediate data* during a power outage. *Configuration data* keeps the functionality of a FPGA chip and *intermediate data* is the data generated during computation. By keeping both, long computations can be achieved by retrieving a checkpoint after power resumes.

The non-volatile memory based FPGAs (NV-FPGAs) are natural candidates to address this challenge. With the substitution of NVMs such as ReRAM, STT-RAM, and PCM for SRAMs, *configuration data* can be retained locally on the chip with benefits of low leakage power, short critical path, and small area, etc [5–10]. Therefore, costs associated with loading *configuration data* from off-chip flash memories are avoided when FPGA recovers from a power outage. In the existing NV-FPGAs and traditional FPGAs, *intermediate data* is held by registers which consist of volatile flip-flops (FF). Like *configuration data*, *intermediate data* needs to be saved during power is lost or weak in order to resume system state after the power comes back. To reserve intermediate data, non-volatile flip-flops (NV-FFs) have been integrated on processors. Such non-volatile processor freezes all registers data locally on the chip if it is shut off [11]. The success of NV-FFs in processors makes it a good candidate for FPGA flip-flop. However, FPGA's register resource is significantly more than the processor's and FPGA resource utilization varies design to design. Freezing all registers on FPGA will waste rare energy in energy harvesting system.

To improve efficiency in preserving *intermediate data* and reducing the roll-back impact from power interrupt, this paper proposes DFT-FPGA, a data flow tracking methodology on FPGA via High-Level-Synthesis (HLS). As HLS takes software functions as inputs and compiles it to Register-Transfer-Level (RTL) design. DFT-FPGA builds data flow trackers for such functions and a control unit to parse trackers' status in HLS. With an offline mapping of functions to trackers, DFT-FPGA can online track the *intermediate data* inside a function via a tracker. Then, instead of all data, only a set of tracked *intermediate data* in registers will be locally stored in non-volatile flip-flops. In this way, the cost to preserve *intermediate data* can be significantly reduced. The main contributions of this work are as follows:

- Design of binary counter based tracker framework which tracks data flow in FPGA.
- Design of control unit which stores the mapping of intermediate data and its on-chip physical address.
- Design of an off-line intermediate data to tracker mapping algorithm.
- Design of function split and merge method for DFT-FPGA.
- A demonstration of the performance of NV-FF based FPGA.
- A demonstration of the efficiency of FPGA design on representative benchmarks.

The rest of the paper is organized as follows. Section 2 presents FPGA in an energy harvesting system, non-volatile FPGA, High-Level-Synthesis, and the motivation of DFT-FPGA. Section 3 presents the DFT-FPGA framework. Section 4 presents the function-to-tracker mapping algorithms and Section 5 presents the evaluation results.

## 2 PRELIMINARY

We will first present FPGA in an energy harvesting system in subsection 2.1. Then works related to NV-FPGA and NV-FF architecture will be presented in subsection 2.1.1. The background of High-Level-Synthesis will be introduced in subsection 2.2 and the motivation of the proposed work will be presented in subsection 2.3.

### 2.1 FPGA and Energy Harvesting System

FPGA is widely adopted in open field applications such as wireless network platforms [12–14]. In this application scenario, the energy harvesting system outperforms other resources such as battery and cable thanks to its perpetual power supply. In energy harvesting systems, ambient energy such as solar, wind, mechanical strain, ambient radiation, and human motion can be harvested to power the energy consumer and its peripheral devices. Though energy harvesting can provide a perpetual power supply, when compared to systems powered by cable, energy harvesting system may only harvest and supply a small amount of energy. Moreover, the passive energy harvesting approach makes the harvested energy unpredictable and unreliable. It is observed that small harvesters such as a wrist-worn motion harvester can provide about  $40 \mu W$  power with worst-case power outages every  $10ms$  in daily activities [15, 16]. Therefore, a device with the energy harvesting system should not only be able to work in a low-energy mode but also be robust enough under intermittent power.

An energy harvesting system usually consists of an energy source, regulator, capacitor, and energy consumer. A classical system is shown in Fig. 1. The regulator is a bridge between ambient energy, energy consumer, and an auxiliary capacitor. Energy consumer is powered by the regulator when harvested energy is sufficient. Meanwhile, the capacitor is fully charged and standby for energy spike or power outage/weak. If the ambient energy becomes weak, the additional energy from capacitor should sustain the consumer’s rest of work or preserve its current state. As the computation complexity varies from application to application, the energy needed for each application are different. Therefore, preserving the current states are widely adopted in designs [17–19, 19–24]. Moreover, the energy from capacitors is limited as the size of capacitors in small scale energy harvesting system can be as small as  $\mu F$  and under  $5v$  [19]. For energy consumers like microcontroller, ASIC, and FPGA, their dynamic power varies from cycle to cycle. Evaluating and recording the energy from each cycle to the end can be unrealistic as a regular application can be thousands or even dozens of thousands cycles.

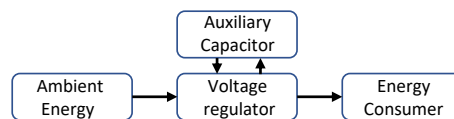


Fig. 1. An energy harvesting system.

**2.1.1 FPGA architecture.** A basic FPGA architecture consists of Configurable Logic Blocks (CLB), Block RAMs (BRAMs), Connect Boxes (CB), Switch Boxes (SB), and Routing Channels which is shown in Fig. 2. Each CLB is an independent computation group and computation results are transmitted via Routing Channels. Switch Boxes redirect the data in Routing Channels to horizontal or vertical channels. BRAMs in FPGA serve as long-term massive data storage during computing. In this way, a CLB can reach any other CLB in FPGA. Computation results can be stored in BRAMs. The breakdown structure of a CLB from Xilinx FPGA is shown in Figure 3 (a). Look Up Table (LUT) is the

smallest programmable computation unit inside a CLB which is wrapped by Basic Logic Element (BLE). As shown in this 4-input LUT, the LUT can have different logic by changing its mask binary order; different combinations of inputs will lead to different results in logic. Each LUT is followed by two flip-flops in a BLE which compose registers to support sequential logic in high-frequency computation. The registers hold the intermediate results from LUTs in each clock cycle. Then, data is sent out of CLB by Connect Box and this data is routed through Switch Boxes and Routing Channels. For a specific application, according to its complexity, a number of LUTs, flip-flops, Switch Boxes, and Routing Channels are selected and activated in FPGA to build its corresponding computation logic and data flow path. (In Xilinx FPGA, a CLB shown in Fig 3 (a) is named as SLICE and two SLICES form a physical CLB)

For traditional FPGA, SRAMs are used to build all these components. SRAMs are usually fast but volatile. Thus, the intrinsic flexibility in reconfiguring makes an FPGA easily switch between applications. However, configuring data and computation data is vanishing from the chip when power is lost or weak. In order to keep the data, part of the FPGA components need to be replaced by non-volatile memory.

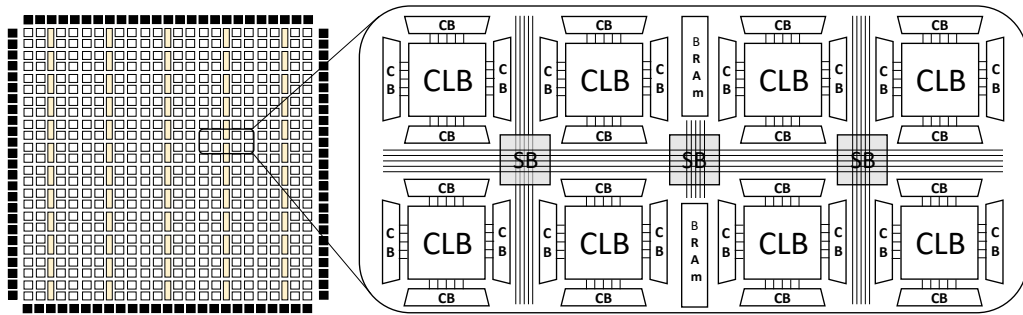


Fig. 2. An overview of FPGA architecture.

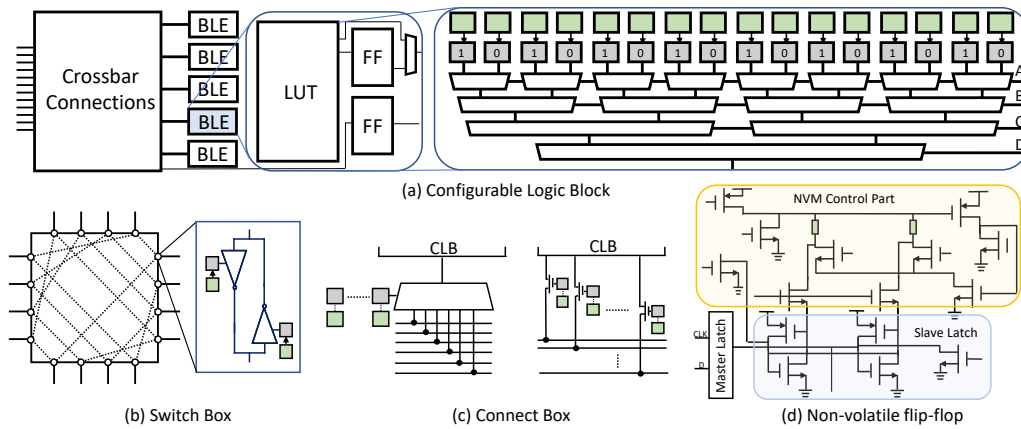


Fig. 3. FPGA breakdown and Non-volatile. FPGA

**2.1.2 Non-volatile FPGA.** The study of non-volatile FPGA has been conducted by Gaillardon, Cong, et, al [25–31]. The existing NV-FPGAs preserve all configuration data on the chip. As the configuration data for LUT, Connect Boxes, and Switch Boxes are stored in SRAMs bit by bit, by replacing configuration data SRAMs with non-volatile memories (NVMs) such as ReRAM and STT-RAM, the configuration data can be permanently retained on FPGA. Though NVMs writing and reading speed is slower than SRAMs, it can preserve its data even power is lost.

Figure. 3 shows how the configuration data SRAMs are replaced by NVMs on-chip [25]. In this figure, a SRAM is represented by a grey block and an NVM is represented by the green block. The LUT configuration data is stored in its mask which is held by SRAMs. After replacing the SRAMs in the mask with NVMs, configuration data for LUT can be permanently preserved on chip after one programming. Figure. 3 (b) and (c) show how to preserve Connect Boxes and Switch Boxes configuration data with NVMs. For Switch Boxes, after configuring all control SRAMs on the connections between horizontal and vertical tracks, data paths inside Routing Channels are formed. For Connect Boxes, a SRAM determines the on/off of a path between a CLB and a track. After configuring all needed Switch Boxes and Connect Boxes, multiple data routing paths are formed. After adopting NVMs, the routing paths in FPGA can also be preserved. Thus, the configuration data for an application can be preserved on-chip even power is off. After programming once, these NVMs can keep all configurations on-chip which avoids duplicate programming for the same program.

SRAM based BRAMs in FPGA can also be directly replaced with non-volatile BRAMs (NV-BRAM). BRAMs are usually working as long-term massive storage on-chip. STT-MRAM based BRAMs (NV-BRAM) are proposed by Ju, et, al [31]. Compared with SRAM BRAMs, NV-BRAMs have higher density and smaller area. When substituting an SRAM with an NVM cell, six transistors are replaced with one NVM cell. Thus, for Switch Boxes, Connect Boxes, LUTs, and BRAMs, they can have a smaller area and be closer to each other in physical distance. In this way, the physical data routing distance is reduced, bringing additional benefits such as higher working frequency and more energy efficiency. Furthermore, NVMs are compatible with CMOS technology via back-end-of-line technique [32]. By growing the NVM cells on the top of the chip, it adds non-volatility to an FPGA without increasing chip area and further reduces the area of FPGA components. An NVM based fully functional FPGA architecture is proposed by Cong, achieving 5.18x area savings, 2.28x speedup and 1.63x power savings compared with regular FPGAs [26].

**2.1.3 Non-volatile flip-flops.** For the intermediate data, it is usually held in registers which are consisted of flip-flops. Non-volatile flip-flops are proposed by Qazi, Bartling, et, al [11, 33–35]. Contrary to configuration data, intermediate data are frequently refreshed and the data flip frequency can be hundreds of mega hertz (MHz). That is, at each clock cycle, the data in a register is refreshed. Therefore, the NVMs writing and reading time may bring delay which hinders the FPGA work frequency. It is observed that a 65nm technology based ReRAM NV-FF has achieved writing time as good as 4μs seconds and 46.2 pico joule per bit [11]. Meanwhile, a regular FPGA usually works at hundreds of MHz, i.e working under ns clock period. With such performance, if NVMs writing happens in NV-FF every clock cycle, the FPGA frequency may be degraded to dozens of MHz.

The architecture of NV-FF is shown in Fig. 3 (d). Based on a master-slave flip-flop, two pieces of NVMs are integrated to its slave logic. By adding extra NVM control part, data in slave logic can be optionally stored into or retrieved from NVM cell. It works like regular flip-flop if NVM writing is not triggered and it can write the data to NVMs or recover data from NVM with a trigger. When writing to NVM is triggered, the clock will be hung and data is written to NVM and vice versa. This avoids the writing to NVMs every clock cycle and the working frequency is not influenced if NVM writing is not triggered. The NVM brings non-volatility but also larger logic area. It is observed in [11] that a NV-FF based processor has an extra 39% area for a single FF but less than 10% extra area for the whole chip. The 39% single FF

area overhead is brought by the NVM’s control logic and the NVM is growing on the top of the chip, which won’t bring extra area. Though NVM writing is not triggered at every clock cycle, the area overhead from the control logic will increase its intrinsic delay and the size of a CLB, leading to bigger FPGA size, which increases the routing distance. This may decrease the FPGA working speed. The impacts on FPGAs working frequency after bringing in NV-FF is evaluated in section 5.

For each NV-FF, it can be triggered to work as regular, store, or retrieve mode. If other FPGA components are non-volatile, by storing the intermediate data to the NVM if power is weak, the chip state can be held on board and be retrieved later. However, selecting a single flip-flop in an FPGA chip is not accessible as a single flip-flop can not be indexed inside a CLB. Moreover, FPGA’s flip-flop resource can number in the thousands and tens of thousands. In the proposed design, selected flip-flops need to be stored in order to keep intermediate data and flip-flop storing and retrieve are executed SLICE by SLICE. This is due to FPGA tools like Vivado packing flip-flops into the same SLICE [36]. A physical CLB in Xilinx FPGA contains two SLICES and each SLICE can be indexed on the chip. In general, 4 LUTs and 8 flip-flops or 8 LUTs and 16 flip-flops are placed in a SLICE. Therefore, the flip-flop write and retrieve are triggered SLICE by SLICE in the proposed design.

In DFT-FPGA, the SLICE addresses are acquired after FPGA synthesis and pre-loaded to FPGA. During online intermediate data tracking, such SLICE addresses can be read out after parsing trackers’ status. Then, the flip-flops in these SLICES can be triggered in writing or retrieving.

## 2.2 High-Level-Synthesis (HLS)

High-Level-Synthesis converts software language such as C/C++ to Hardware Description Language (HDL) like Verilog and VHDL. HLS’s efficiency and accuracy has been verified in modern FPGA applications [37–40]. It takes software functions  $F$  as inputs to generate HDL modules  $M$  and state transition flow  $S$ . After HLS, a program is split into multiple modules according to program hierarchy. These modules are interpreted as different states in the state transition control. State transition control initializes and terminates the modules during FPGA operation. In HLS, each function under top function is generally compiled to a standalone module. Based on the data dependency between modules (functions), these modules are triggered in parallel or sequential in state transition control. A basic HLS FPGA design with its data flow control is shown in Fig. 4 [41].

In this program, there are three functions  $F_1$ ,  $F_2$  and  $F_3$  under top function  $F_{main}$ . After HLS, functions are converted to modules as shown in Fig. 4 (a). In the top function,  $F_1$  and  $F_2$  have data dependency and  $F_3$  is independent of  $F_1$  and  $F_2$ . Therefore, as shown in Fig. 4 (b) state transition control,  $F_2$  has to be placed after  $F_1$  in state flow  $S$ . Meanwhile,  $F_3$  can start with  $F_1$ . In states  $S_1$ ,  $S_2$  and  $S_3$ , component information in module  $M_1$ ,  $M_2$  and  $M_3$  such as module names, registers, connections, and cycles can be collected. An unroll of  $S_2$  is shown in Figure. 4 (c). For HLS tools like Vivado/LegUp, it maps module components to different clock cycles and indicates the data flow among clock cycles. In the real case, a state like  $f_2$  may contain sub-state, each sub-state can be unrolled according to clock cycles.

After High-Level-Synthesis, synthesis turns HDL into the implementation of logical gates, BRAMs, and registers. It also indicates the physical placement of all modules components. After implementation, these components are mapped to different SLICES. The address of these SLICES is generally represented as 2-dimension  $X_{xx}Y_{yy}$  [36].

The proposed design utilizes state transition control after HLS and module components placement after synthesis. By analyzing the state transition, DFT-FPGA builds cycle accurate data tracker for each software function. After synthesis,

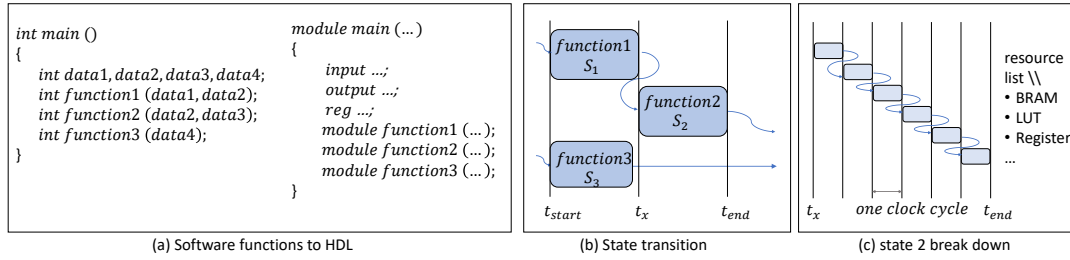


Fig. 4. High-Level-Synthesis.

SLICE addresses related to different registers are acquired. By online reading the status of trackers and parsing it to SLICE address, the SLICES holding the intermediate data can be selected and saved.

The work flow of DFT-FPGA is shown in the Figure. 5. HLS first generates the state transition and state components information. Tracker generation builds tracker framework accordingly. After tracker generation, the source function combined with tracker design are HLSed one more time. Then, *synthesis* generates the executable bitstream and provides all SLICE address  $X_{xx}Y_{yy}$ . After programming FPGA, DFT-FPGA pre-loads the SLICE addresses to FPGA and starts the computation. The DFT-FPGA framework will be presented in Section 3 and the off-line analysis algorithm will be presented in Section 4.

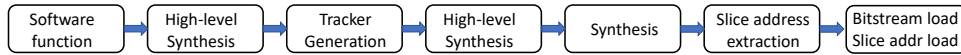


Fig. 5. DFT-FPGA work flow.

### 2.3 Motivation

Existing designs preserve chip state by placing checkpoints in computation [17–19, 22–24, 42]. Azalia et al. propose *Chime*, which places checkpoints in Register-Transfer-Level (RTL) design. *Chime* off-line analyzes the forward computing cost and back-up overhead to determine checkpoint placement. By placing checkpoint in different locations, the computation can recover from a near checkpoint if a power outage happens. Yuan et al. propose *CP-FPGA*, a framework that based on HLS result. It places the different states of the main function in different BRAM-based (block RAM) physical areas by modifying FPGA synthesis algorithm. Each state result is stored in its dedicated BRAM and when power is lost in the mid of a state, the computation can start from its previous state. In the existing works, the intermediate data back-up is triggered at every checkpoint. After retrieving from a checkpoint, the computation can continue. While the prior strategies can successfully preserve the intermediate data, long roll-back can easily occur if power is lost in a long state. This case is shown in Fig. 6 (a), a dot represents the end of a state. Checkpoints are placed at each dot. For applications with a long state, such strategies may be hard to complete the computation if a power outage happens in the middle of a long state. Roll-back may occur several times inside a long state until power is stable. Moreover, by tying a state and a BRAM together, BRAM resources can be insufficient for a large program with multiple states, and periodical data back-up happens even if power is stable.

Fig 6 (b) shows the performance comparison between proposed design and periodical checkpoint design; the red line shows checkpoint technology and the green line shows DFT-FPGA. Power outage happens at  $t_3$  and  $t_7$ . Checkpoints

are placed at progress 20%, 40% and 60%. As checkpoints are pre-defined, data writing occurs at each checkpoint regardless of the power condition. The computation starts from its previous checkpoint after power loss. However, in DFT-FPGA, the checkpoint is avoided and data flow is always tracked. Thus, data back-up happens only if power is lost and computation starts from the progress where power breaks. Compared with DFT-FPGA, the existing checkpoint placement technologies for FPGA in energy harvesting system suffer from long roll-back time, increasing the complexity of original program, and modifying the FPGA synthesis algorithm.

Preserving the data for the entire chip may also be an option [11]. By triggering writing and retrieving of flip-flops in all FPGA SLICES, all the data on chip can be fully reserved. However, such strategy can be heavily resource intensive. As FPGA resource utilization varies from design to design, preserving the entire chip causes unnecessary NVM cell writing in unused memories, which will waste rare harvested energy and slow down the writing speed. As it is shown in Figure. 6 (c), this computation only occupies 15% of the chip resource, the remaining 85% components are still stored and retrieved if preserving the whole chip data. After applying DFT-FPGA, unnecessary back-up can be avoided. The benefits and impact after applying DFT-FPGA will be presented in section 5.

Our previous work FC-FPGA applies shift-register like data flow tracker to locate and retrieve intermediate data in RTL level [43]. In this work, binary counters are adopted to further reduce resource utilization and a full High-Level-Synthesis based work flow is proposed, which significantly reduces the workload.

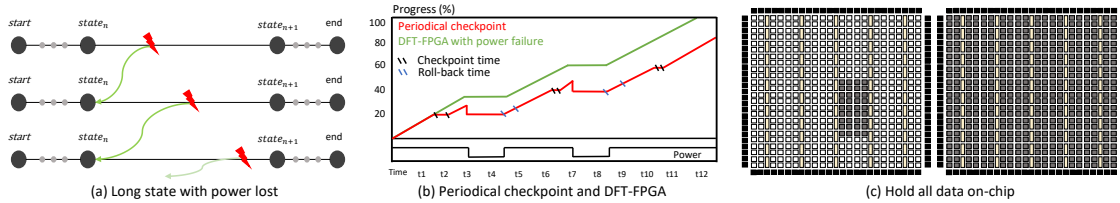


Fig. 6. The motivation example.

### 3 DFT-FPGA FRAMEWORK

The proposed DFT-FPGA methodology includes both framework and data-to-tracker mapping algorithm designs. In this section, we will introduce the framework of DFT-FPGA. The algorithms that work with the framework will be introduced in Section 4.

#### 3.1 Hardware Architecture Overview

The proposed design includes function trackers  $f$  and NV-FF control unit  $CU$  which is shown in Figure 8 (b). In this figure, a finite state machine is generated by HLS in the back-end to control data transition in functions, i.e. state transition between states. Each function is assigned a function tracker. Trackers are read by the control unit which pre-loads SLICE addresses and maps them to associated registers. In DFT-FPGA, at every power outage, the control unit reads function tracker's status and then select the corresponding SLICE to trigger action. In the proposed design, the control path to NV-FF control part is considered already embedded in NV-FPGA.

### 3.2 Function Trackers

As all intermediate data is held by registers, function trackers are designed to track the active registers at each clock cycle. Therefore, a tracker is built to have the same clock cycles with its corresponding function. By reading tracker's status, the data flow location in its function can be acquired.

In DFT-FPGA, each function is assigned a function tracker to trace its data flow. The tracker is activated simultaneously with its corresponding function and they are terminated at the same time. The method to insert trackers to a software program is shown in Figure. 7 (a). Functions  $F_1$ ,  $F_2$ , and  $F_3$  under  $F_{main}$  are assigned private trackers  $f_1$ ,  $f_2$ , and  $f_3$ . The state transition and timing among  $F_{1-3}$  is as it is illustrated in Fig. 4 (b). Therefore, the initialization of trackers  $f_{1-3}$  should also follow such orders. In the proposed design, *lock* is utilized between trackers to keep trackers initialized in the right order. The *lock* in a tracker consists *lock<sub>head</sub>* and *lock<sub>tail</sub>*. If a tracker is initialized after its anterior tracker, its *lock<sub>head</sub>* is the *lock<sub>tail</sub>* of the anterior tracker. As shown in Fig. 7 (c), tracker  $f_2$ 's *lock<sub>head</sub>* is  $f_1$ 's *lock<sub>tail</sub>*. After tracker  $f_1$  is terminated, *lock<sub>tail</sub>* is set to be 1. Thus, tracker  $f_2$  is always blocked if  $F_1$  and  $f_1$  are not finished. As there is no data dependency between function  $F_1$  and tracker  $f_1$ ,  $f_1$  can start with function  $F_1$  simultaneously. For trackers which start with the beginning function, such as  $f_1$ , its *lock<sub>head</sub>* is pre-defined to be 1 to unblock itself. In this way, all trackers can be initialized and terminated with their corresponding functions.

A function tracker consists of loop arbitration  $t$ , binary counter *count*, tracker status register  $f_{status}$ , and tracker lock *lock<sub>head</sub>* *lock<sub>tail</sub>*. Without loss of generality, trackers can track function with loops or with regular operations. An example of a function and its tracker logic is shown in Fig. 7 (b) and (c). This is a function with an outer loop and an inner loop. In the tracker, the first loop  $t$  handles functions with loops. Loop iterations  $t$  corresponds to the outer loop iteration number in a function.  $Count_{max}$  is the length of all operations under function's outer loop. The binary counter increments to  $count_{max}$  and then be reset to zero for the next outer loop iteration. Thus, the binary counter can be reused in all outer loop iterations. If a function does not contain any loop,  $t$  is set to one and  $count_{max}$  is the length of the function. When power is lost during computing, the energy harvesting system sends  $P_{loss} = 1$  to DFT-FPGA. With  $P_{loss|resume} = 1$ , the tracker sends out its status *count* as  $f_{status}$ . Trackers'  $f_{status}$  will be further parsed by control unit. When reaching the end of tracking, the  $f_{status}$  is reset to zero. In this way, the tracker can count with the function process and send out the process stage when power is loss. After power resumes  $P_{resume}$ , trackers data is recovered by NV-FPGA first and the resumed trackers' status are utilized to wake up the stored intermediate data.

To further reduce the binary size, the binary counter can be defined to lower bit-width such as 4bit, 8bit, and 16bit according to the length of a function. In most cases, the binary counter size is found to be small as 4-8 bit (tracking length ranges 225-65025 cycles). The resource utilization, tracking length, and performance of trackers in different sizes will be discussed in section 5.

### 3.3 NV-FF Control Unit

The control unit read all trackers' status  $f_{status}$ . As trackers' status is cycle accurate, by keeping the active register SLICE address for each clock cycle in control unit, DFT-FPGA can acquire the physical location of intermediate data flow. Such address can then be utilized by NV-FPGA to have SLICE registers data stored or retrieved.

The control unit also keeps the mapping relations of function trackers status and registers' SLICE address. It consists of one or multiple BRAMs and address look-up logic as shown in Figure. 8 (a). All associated SLICE addresses for trackers are pre-loaded to  $cu_{BRAM}$  with index  $f_{status} + offset$ . *Offset* works as index boundary in  $cu_{BRAM}$  when a new tracker is generated. And each  $cu_{BRAM}[offset]$  is pre-set to zero. Thus, each tracker can have a certain range

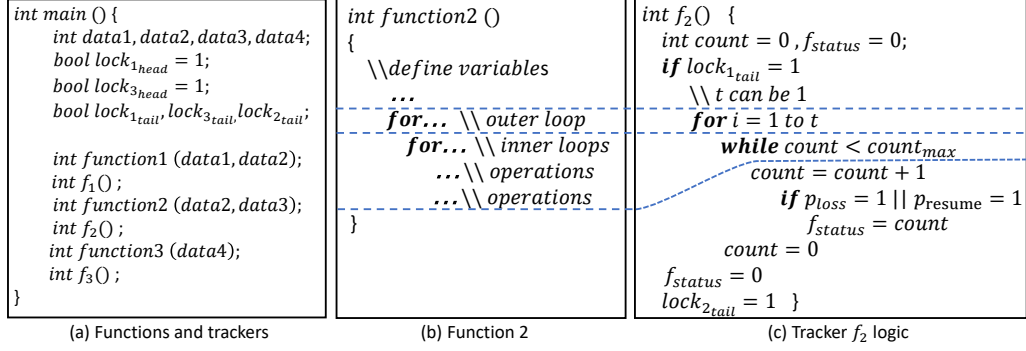


Fig. 7. Tracker design and assignment in HLS

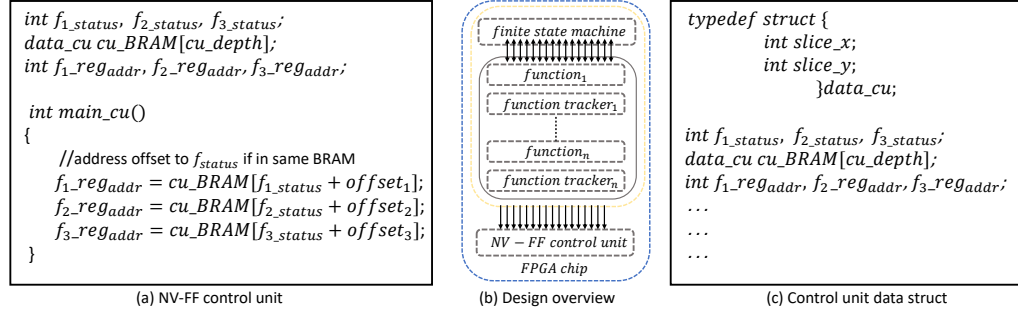


Fig. 8. Control Unit and DFT-FPGA overview.

of storage in  $cu_{BRAM}$ . In this figure, all trackers  $f_{status}$  is combined with offset including the first tracker  $f_1$ . This is because trackers themselves in DFT-FPGA are needed to be reserved as well,  $cu_{BRAM}$  keeps trackers SLICE address with index zero to  $offset_1$ . The SLICES where trackers are placed are always stored when power is lost. By online reading  $f_{status}$ , corresponding SLICE addresses are parsed by the control unit. SLICE storing or retrieving can then be operated on these SLICES. As tracker  $f_{status}$  is zero if it is not triggered or terminated, no action to SLICES will be executed for such trackers and the control unit will parse zero addresses.

In DFT-FPGA, one BRAM  $cu_{BRAM}$  is instantiated to keep all trackers' mapped SLICE addresses. During HLS, if the depth of the  $cu_{BRAM}$  is too big to be placed in a single physical BRAM, the synthesis tool will automatically expand it to multi-BRAM. As the SLICE address in FPGA is organized as  $X_{xx} Y_{yy}$ , a data structure is used in DFT-FPGA to keep address in  $X$  and  $Y$  direction which is shown in Figure. 8 (c). The resource utilization and performance of the control unit will be discussed in section 5.

After assigning trackers to functions, there are two tasks that need to be accomplished before DFT-FPGA can work properly. First of all, for a given program with multiple functions, we need to identify which registers will keep intermediate data at a certain clock cycle in each function. Second, as tracker assignment is arranged according to function hierarchy, the main function should only contain the substantiation of functions. In this task, function merge and function split will be discussed.

## 4 DFT-FPGA OFF-LINE ANALYSIS

In previous sections, we show how to generate and assign trackers to functions. In this section, we will present how to establish mappings between a function and its tracker, and how to merge or split functions in a program.

### 4.1 Function to Tracker Mapping

After analyzing the program hierarchy and the state transition, the activation of trackers are determined. The mapping of tracker status to data flow in a function can be determined by unrolling a function's state. A state breakdown is shown in Figure 9 (a). In this figure, rectangle blocks represent operations inside the function and they are arranged to clock cycles from  $t_{start}$  to  $t_{end}$ . At each clock cycle  $t_n$ , operations  $p_{t_n}$  with its register  $reg_{t_n}$  are placed. The connecting arrows indicate the data flow inside a state. In this figure,  $p_2$  and  $p_3$  are operations for  $p_{t_{n+2}}$ ;  $reg_2$  and  $reg_3$  are registers for  $reg_{t_{n+2}}$ . Every operation is followed by its register to get its data held at every clock cycle. For registers  $reg_{t_n}$  in a state, they keep the intermediate data within a function at different clock cycles. Those registers are the target to be tracked by trackers defined with  $checkpoint_{t_n}$ . As different registers are triggered during the function process, registers that hold intermediate data for each clock cycle should be determined and those registers' SLICE addresses are stored by the control unit.

In FPGA design, operations can execute in parallel like  $p_2$  and  $p_3$ . And operations may have multi-cycle length such as  $p_4$ . Therefore, at certain clock cycle, there can be multiple registers  $reg_{t_n}$  or previous register  $reg_{t_{n'}}$  to hold the intermediate data. The method to determine  $checkpoint_{t_n}$  is illustrated in Algorithm 1. At each cycle  $t_n$ , its register  $reg_{t_n}$  is added to  $checkpoint_{t_n}$  because its operations end at this cycle. If a multi-cycle operation is cross  $t_n$  which starts at  $t_{n'}$  and ends at  $t_{n''}$ , the  $reg_{t_{n'}}$  ahead of this operation is also added to  $checkpoint_{t_n}$ , e.g.  $checkpoint_{t_{n+2}} = reg_2 \cup reg_3$ ;  $checkpoint_{t_{n+3}} = reg_2 \cup reg_3$ . In this way, the registers holding intermediate data for each clock cycle are acquired. For multi-cycle operation like  $p_4$  at  $t_{n+3}$ , DFT-FPGA inserts roll-back logic to ensure the consistency between tracker and function after retrieve. The roll-back logic is shown in Fig. 9 (b). After applying Algorithm 1 to all functions and trackers, the mappings between registers to tracker status is established.

If this is a loop function as indicated by the dashed line in Fig. 9 (a),  $t_{start}$  to  $t_{end}$  is tracked by  $count$  and its loop iteration is controlled by  $t$  in tracker. The same binary counter  $count$  will be called  $t$  times. In this way, DFT-FPGA can scale down the binary counter size and save more flip-flop resources. By analyzing one iteration's mapping relation, the mapping for the whole function is acquired. During synthesis, these registers' SLICE address can be acquired. After that, the mappings between trackers status and SLICE address can be established. Then, applying the mapping algorithm, registers are mapped to tracker. However, for registers barren computation, DFT-FPGA can choose to not assign tracker to if tracker flip-flop resources are more than target registers. Such cases are studied in section 5.

After analyzing the mapping between a tracker and its function, the trackers for the main function  $F_{main}$  need to be arranged. The proposed DFT-FPGA will tune the hierarchy of  $F_{main}$  to make it suitable for tracker assignment. The next task includes function split and function forming.

### 4.2 Function Split and Merge

**4.2.1 Function Split.** As software language is normally flexible in hierarchy and coding style. A program's hierarchy may need to be tuned and then DFT-FPGA can be applied. A function needs to be split if there are independent loops or operations aside of a loop. Such a case is shown in Figure 10 (a) and (b). For independent loops as shown in Fig. 10 (a), the function is split according to outer loops. As the tracker in DFT-FPGA is designed to track one outer loop with

**Algorithm 1**  $Checkpoint_t$  determination

---

Input: function state  $S$ , start point  $t_{start}$ , end point  $t_{end}$ , operations  $p_{t_n}$ , registers  $reg_{t_n}$   
Output:  $checkpoint_t$   
Define:  $start < n < end$ ,  $start < n' < n$ ,  $n < n^* < end$   
**for**  $t_n \in S$  **do**  
   $checkpoint_t.append(reg_{t_n})$   
  **for**  $t_{n'} \in S$  **do**  
    **for**  $t_{n^*} \in S$  **do**  
      **if**  $reg_{t_{n'}} \diamond p_{t_{n^*}} = 1$  **then**  
         $checkpoint_t.append(reg_{t_{n'}}) \setminus \setminus \diamond$   
      **end if**  
    **end for**  
  **end for**  
**end for**  
**return**  $checkpoint_t$

---

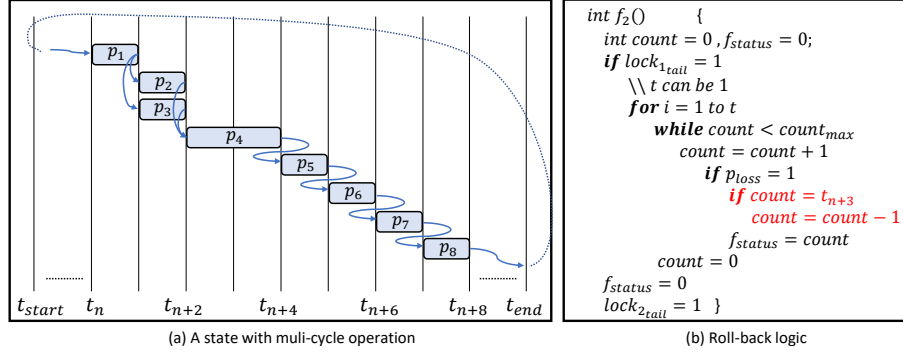


Fig. 9. A state breakdown and roll-back logic.

its all inner operations, a function is split to multiple functions according to the number of independent loops. Then, trackers will be assigned to split functions. If a function contains more than loop functions, the function needs to be split based on the boundaries between loop and other operations. A case where a loop is followed by other operations is shown in Fig. 10 (b). It needs to be split into two functions. Through splitting functions, the proposed tracker logic can be successfully applied.

**4.2.2 Function Merge.** Under the main function, there can be operations between functions. As the state transition is arranged between functions, those non-function operations will be automatically merged into a function by HLS. This will cause obfuscation in function-to-tracker mapping and the auto-merged function cannot be directly applied with trackers. Such a case is shown in Fig 11. By wrapping these operations to a function, state transition can be arranged in different functions. Then, trackers can be built and assigned to all tuned functions.

## 5 EXPERIMENT

In this section, we first evaluate the performance of FPGA architecture with NV-FF in subsection 5.1. Second, we evaluate the proposed tracker and control unit resource utilization and performance in subsection 5.2. Third, we evaluate the resource utilization and performance after applying the proposed DFT-FPGA on different benchmarks in

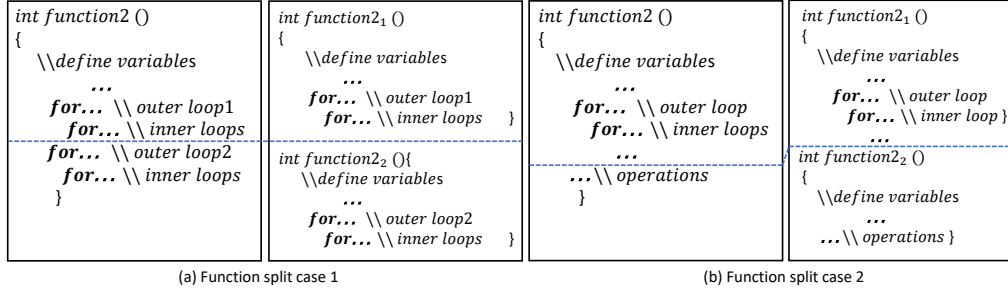


Fig. 10. Function split.

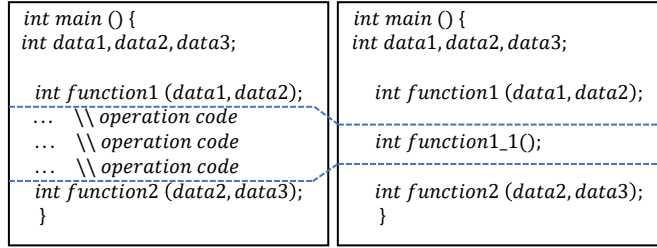


Fig. 11. Function merge.

subsection 5.3. Last we evaluate the performance comparison between the periodical checkpoint and the proposed design in subsection 5.4. In experiments, tool Verilog-To-Routing (VTR) is used in evaluating the FPGA architecture with NV-FF in subsection 5.1. Vivado HLS is used in remaining evaluations for analyzing and generating DFT-FPGA and analyzing benchmarks. Vivado is used in FPGA synthesis and getting all registers SLICE address.

### 5.1 NV-FF FPGA performance

In this subsection, we base on FPGA architecture *K6-frac-N10-mem32K-40nm* from VTR, by adding delay to its D flip-flop module and increasing CLB area to evaluate the impact from NV-FFs. As presented in section 2.1.3, the control part in NV-FF brings extra area. Increasing the area of a single flip-flop can degrade its timing performance but flip-flop area size is not simulated in VTR. Therefore, we add extra delay to each single flip-flop according to the area scaling up ratio 39% and 49% [11, 44]. The extra 39% case is caused by additional 15T2R, which is 15 transistors and 2 ReRAMs [11]. The extra 49% case is caused by additional 22T2R, which is 22 transistors and 2 ReRAMs [44]. The increase of flip-flop size also brings a larger CLB area, which will lead to longer routing distance and may degrade FPGA's working frequency. In the evaluated FPGA architecture, each CLB contains 10 flip-flops. For the two types of NV-FF structure, due to VTR adopts *minimum width transistor area* [45] to define the size of components, we increase the CLB size by 15 *minimum width transistor area* and 22 *minimum width transistor area* accordingly. The FPGA architecture size increment is shown in Figure 12 (a). In this figure, the blue column represents the base architecture, the orange column represents the 15T2R architecture, and the grey column represents the 22T2R architecture. We observe a 0.2% logic area increasing from base to 15T2R and 0.07% from 15T2R to 22T2R. Routing area increases 0.16% from base to 15T2R and 0.04% from 15T2R to 22T2R.

To evaluate the impact on FPGA working frequency which suffers from longer flip-flop delay and routing distance, we apply seven benchmarks in VTR on three FPGA architectures, respectively. The critical path delay and maximum working frequency are shown in Fig. 12 (b) and (c). In the evaluated benchmarks, we observe that 15T2R architecture causes less than 3% of additional critical path delay and 22T2R architecture causes less than 7.4% additional critical path delay compared to base architecture. As the critical path delay determined the maximum working frequency, we also show the maximum working frequency in Fig. 12 (c). We can observe that less than 6.5MHz degradation is caused by 15T2R and less than 10MHz is caused by 22T2R. From the evaluation, we can see that integrating NV-FF on FPGA brings a bit performance degradation, i.e, several MHz. However, as most designs running on FPGA work at hundreds of MHz [37, 39, 46, 47], such degradation has little impact on overall performance and achieves non-volatility of flip-flops.

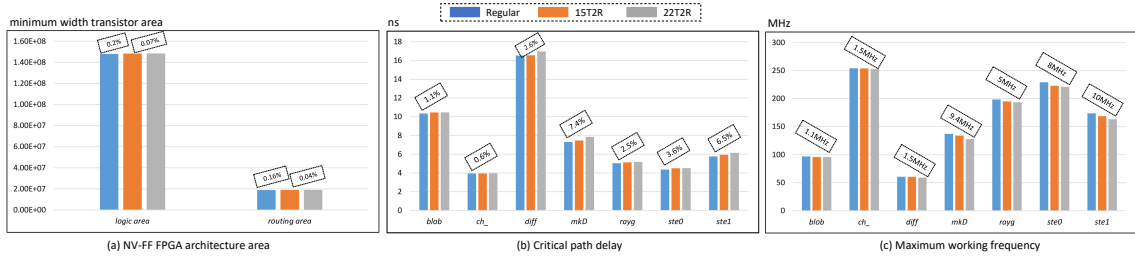


Fig. 12. NV-FPGA performance.

## 5.2 Tracker and Control Unit Evaluation

In the previous section, we evaluated the performance of NV-FF based FPGA architecture. In this section, we will evaluate the resource utilization and timing performance of DFT-FPGA framework. The evaluation is based on FPGA chip *xc7z020clg484*. Table 1 shows the flip-flop, LUTs usages, and maximum tracking cycles when a tracker size scales from 4bit to 9bit. The resource of *xc7z020clg484* is also listed. In the evaluation, we observe less than 0.03% of flip-flops and less than 0.21% LUTs are used to build a tracker. Similarly, less than 0.05% of flip-flops and less than 0.31% LUTs are used to build a control unit. If applying DFT-FPGA on large scale FPGAs, the utilization ratio will be further reduced. The maximum tracking cycles are  $Max\ Cycle = t * count_{max}$  which is illustrated in in section 3.2. For example, 8-bit tracker can count a function with up to  $65025 = 255 * 255$  cycles.

The control unit keeps SLICE addresses and indexes it after reading trackers' status. The control unit's resource utilization is shown in Table 2. In this table, we show the resource of a control unit with one tracker when tracker size scales from 4bit to 9bit. A  $n\ bit$  counter needs  $count_{max}$  depth in BRAM to store SLICE address because the  $count$  start over when enter each iteration of  $t$ . Thus, the depth needed for a tracker is much smaller than the length of a function. When the counter is less than 8bit, Vivado HLS optimizes it into flip-flops and LUTs to save BRAM resource.

The timing performance of a DFT-FPGA framework is shown in Table 3. In this evaluation, we measure the maximum working frequency of 8-bit standalone tracker, standalone control unit, and DFT-FPGA which is an integration of one 8-bit tracker and control unit. We can observe that a standalone tracker can work up to 500MHz and a standalone control unit can work up to 400MHz on FPGA *xc7z020clg484*. With the evaluated NV-FF FPGA performance and the DFT-FPGA performance, we can conclude that the DFT-FPGA consumes a small amount of FPGA resources and will not be the speed bottleneck after being applied to the source program.

Table 1. Tracker Resource Utilization

Tracker size	4bit	5bit	6bit	7bit	8bit	9bit	FPGA
FFs	15	18	21	24	27	30(0.03%)	106400
LUTs	90	102	102	102	102	110(0.21%)	53200
Max Cycle	225	961	3969	16129	65025	261121	-

Table 2. Control Unit Resource Utilization

Tracker size	4bit	5bit	6bit	7bit	8bit	9bit	FPGA
FFs	52	52	52	52(0.05%)	36	36	106400
LUTs	138	142	150	166(0.31%)	134	134	53200
BRAM	~	~	~	~	2	2	280

Table 3. DFT-FPGA Working Frequency

Frequency	100MHz	150MHz	200MHz	400MHz	450MHz	500MHz	600MHz
Tracker	√	√	√	√	√	√	×
Control Unit	√	√	√	√	×	×	×
DFT-FPGA	√	√	√	√	×	×	×

### 5.3 DFT-FPGA Case study

In the previous section, we showed the performance of a tracker, a control unit and an individual DFT-FPGA framework. In this section, we evaluate the performance of HLS benchmarks from *CHStone* [48] on FPGA *xc7z020clg484* with/without applying DFT-FPGA under 400 MHz working frequency. The benchmarks cover large size benchmark such as *adpcm* and small size benchmark such as *struct*. Table 4 and 5 show the resource utilization of source benchmarks and benchmarks applied DFT-FPGA (DFT). In the table, resources such as BRAM, DSP, flip-flop, LUT, and SLICE are listed. For the source benchmarks, the resource usage and utilization level are presented. For DFT-FPGA, its resource usage includes source benchmark and the applied DFT-FPGA framework. The resource usage and utilization level increment are shown in the table for DFT-FPGA. For benchmarks with higher resource utilization, such as *adpcm*, *aes*, *gsm*, and *float*, a less than 1.5% resource increment is observed. DFT-FPGA generates trackers and control unit to track their data flow. For small benchmarks such as *global* and *struct*, less than 0.3% resource increment is observed. Such benchmarks consume a small number of flip-flops and LUTs, which is even less than its tracker’s resource requirement. For such benchmarks, DFT-FPGA only generates control unit to keep all associated SLICE addresses and save all data. In this way, DFT-FPGA achieves resource efficiency in different sizes of benchmarks. The proposed design shows good adaptability when source programs’ size scales up and scales down. It consumes a small number of FPGA resources to achieve intermediate data tracking in the analyzed benchmarks.

Table 4. DFT-FPGA in Different Benchmarks

Benchmarks	adpcm		aes		gsm		FPGA
	source	DFT	source	DFT	source	DFT	
BRAM	14(5%)	16 (+0.7%)	9(3%)	11 (+0.07%)	7(2.5%)	9 (+0.7%)	280
DSP	114(51.8%)	114(+0%)	0(0%)	0(+0%)	46(20.9%)	46(+0%)	220
FF	3464(3.3%)	3769 (+0.28%)	1028(0.96%)	1321 (+0.28%)	1435(1.3%)	1682 (+0.23%)	106400
LUT	8293(15.6%)	8928 (+1.2%)	4552(8.6%)	5330 (+1.5%)	3903(7.3%)	4487 (+1%)	53200
SLICE	-	472	-	166	-	211	13300

Table 5. DFT-FPGA in Different Benchmarks

Benchmarks	float		global		struct		FPGA
	source	DFT	source	DFT	source	DFT	
BRAM	14(5%)	16 (+0.7%)	3(1%)	3 (+0%)	4(1.4%)	4(+0%)	280
DSP	14(6.4%)	14(+0%)	0(0%)	0(+0%)	0(0%)	0(+0%)	220
FF	2997(2.8%)	3210 (+0.2%)	74(0.07%)	284 (+0.19%)	58(0.05%)	267 (+0.19%)	106400
LUT	4901(9.2%)	5150 (+0.47%)	713(1.3%)	882 (+0.3%)	228(0.4%)	380 (+0.28%)	53200
SLICE	-	402	-	36	-	34	13300

#### 5.4 Comparison DFT-FPGA with Checkpoint Technology

In the previous section, we evaluated the resource utilization of DFT-FPGA in different benchmarks. In this section, we will present the comparison between DFT-FPGA and periodical checkpoint CP-FPGA in resource, roll-back time, and flip-flop storing under different power conditions.

As CP-FPGA places checkpoints at the end of all states and saves checkpoint to a BRAM, the number of extra BRAMs brought by CP-FPGA equals the number of states in a benchmark. In the proposed design, the extra BRAM is brought by control unit, which stores SLICE addresses. In table 6, we show the number of states in each benchmark and BRAM utilization in DFT-FPGA and CP-FPGA. In FPGA *xc7z020clg484*, a single BRAM stores 18Kb data. As shown in the table, the BRAM resource is significantly decreased in DFT-FPGA. This is because the BRAM in DFT-FPGA is generated according to the number of SLICES needed to be tracked. Each BRAM in DFT-FPGA is fully utilized. BRAM in CP-FPGA can not be fully utilized as it is assigned by state number, regardless of the size of state result.

Table 6. BRAM usage in DFT-FPGA and CP-FPGA

Benchmarks	adpcm	aes	gsm	float	global	struct
states	24	8	13	1	3	2
BRAM.DFT	2	2	2	2	0	0
BRAM.CP	24(12x)	8(4x)	13(6.5x)	1	3(3x)	2(2x)

The roll-back time and the number of stored flip-flops in different benchmarks are shown in Figure 13 and Figure 14. In Fig. 13, the x-axis shows the number of power lost during benchmarks running and the y-axis shows the roll-back clock cycles. Power lost is randomly triggered within a benchmark’s computation length, e.g at power lost is 5, there are 5 power lost during computing and every power lost is randomly triggered. In the evaluation, we simulate the number of power lost from 1 to 10 during the computation to mimic different power conditions. Without loss of generality, for each power lost case, we record the result of its mean of 10 test rounds. As shown in the figure, the roll-back time for the proposed design is near zero in all benchmarks and all power conditions. Our performance is not influenced even if power condition is worse. This is because the data flow inside each state is aware by DFT-FPGA; DFT-FPGA can retrieve computation from where it is interrupted. For CP-FPGA, it needs to find its nearest checkpoint and recover from that point. If the length of states is long in benchmarks, the interval between two checkpoints is far from each other. It causes long roll-back if power is lost during the middle of such state. This is observed in the *gsm* benchmark which consists of multiple states with over one thousand cycles each. When power lost occurs in one of such states, long roll-back happens. The performance of periodical placing checkpoint technology is significantly influenced by the source program and power condition. Meanwhile, the proposed DFT-FPGA shows good adaptability in minimized roll-back time for different benchmarks in different power conditions.

Figure 14 shows the stored flip-flop data for benchmarks in different power conditions. In this figure, we record the number of flip-flops that are stored in CP-FPGA and the proposed design. The x-axis shows the power lost case

ranging from 1 to 10. The y-axis shows the number of flip-flops that are stored after finishing computation. As CP-FPGA periodically places checkpoints in design, the number of flip-flops stored is a constant in all power conditions. After a state is called, it stores its state result data in registers to BRAM as a checkpoint. It leads to unnecessary data storing when power lost happens occasionally such as once or twice in computation. For DFT-FPGA, the number of flip-flops which is saved consists of both intermediate data registers and trackers' flip-flop resources. We can observe linear increasing in flip-flops when the number of power lost becomes worse. This is because the data storage in DFT-FPGA happens only at power lost. Periodical placing checkpoint may have fewer flip-flops usages if a small number of checkpoints are placed. Such as *truct*, it is arranged to several long states. CP-FPGA have less flip-flop storing in such benchmarks. However, it brings long roll-back time as shown in Fig. 13.

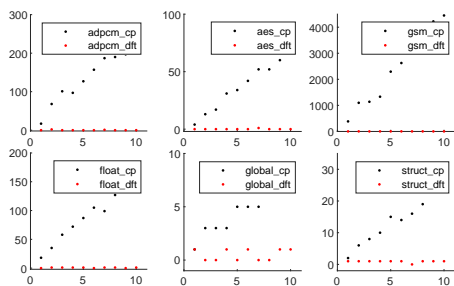


Fig. 13. Roll-back time in CP-FPGA and DFT-FPGA.

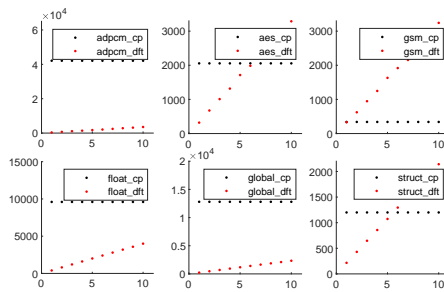


Fig. 14. Flip-flop operations in CP-FPGA and DFT-FPGA.

## 6 CONCLUSION

We propose a data-flow tracking framework, DFT-FPGA, for non-volatile FPGA. It is a full High-Level-Synthesis based framework targeting non-volatile FPGA that can online track and locate the physical location of intermediate data. By parsing, storing, and retrieving certain area of FPGA SLICE, the proposed design can assist NV-FPGA in intermittent computing with minimum resource overhead. The proposed DFT-FPGA also shows good adaptability in different benchmarks under various power conditions with better resource utilization and less roll-back time.

## 7 ACKNOWLEDGEMENTS

This work was supported in part by the National Science Foundation under Grant CCF-1820537, in part by the National Natural Science Foundation of China under Grant 61934005, in part by the National Natural Science Foundation of China under Grant 61674094, in part by the National Science Foundation under Grant CCF-1527464, and in part by the Research Grants Council of the Hong Kong Special Administrative Region, China under Grant CityU 11278316.

## REFERENCES

- [1] Xiaowei Xu, Yukun Ding, Sharon Xiaobo Hu, Michael Niemier, Jason Cong, Yu Hu, and Yiyu Shi. Scaling for edge inference of deep neural networks. *Nature Electronics*, 1(4):216, 2018.
- [2] Xiaowei Xu, Qing Lu, Tianchen Wang, Jinglan Liu, Cheng Zhuo, Xiaobo Sharon Hu, and Yiyu Shi. Edge segmentation: Empowering mobile telemedicine with compressed cellular neural networks. In *Proceedings of the 36th International Conference on Computer-Aided Design*, pages 880–887. IEEE Press, 2017.
- [3] Xiaowei Xu, Dewen Zeng, Wenyao Xu, Yiyu Shi, and Yu Hu. An efficient memristor-based distance accelerator for time series data mining on data centers. In *2017 54th ACM/EDAC/IEEE Design Automation Conference (DAC)*, pages 1–6. IEEE, 2017.

- [4] Lattice. [ice40 lp/hx/lm. lattice](#), 2017.
- [5] Xifan Tang, Pierre-Emmanuel Gaillardon, and Giovanni De Micheli. A high-performance low-power near-vt rram-based fpga. In 2014 International Conference on Field-Programmable Technology (FPT), pages 207–214. IEEE, 2014.
- [6] Xifan Tang, Gain Kim, Pierre-Emmanuel Gaillardon, and Giovanni De Micheli. A study on the programming structures for rram-based fpga architectures. IEEE Transactions on Circuits and Systems I: Regular Papers, 63(4):503–516, 2016.
- [7] Weisheng Zhao, Eric Belhaire, Claude Chappert, and Pascale Mazoyer. Spin transfer torque (stt)-mram-based runtime reconfiguration fpga circuit. ACM Transactions on Embedded Computing Systems (TECS), 9(2):14, 2009.
- [8] Xiaochen Guo, Engin Ipek, and Tolga Soyata. Resistive computation: avoiding the power wall with low-leakage, stt-mram based computing. In ACM SIGARCH Computer Architecture News, volume 38, pages 371–382. ACM, 2010.
- [9] Pierre-Emmanuel Gaillardon, M Haykel Ben-Jamaa, Marina Reyboz, Giovanni Betti Beneventi, Fabien Clermidy, Luca Perniola, and Ian O’Connor. Phase-change-memory-based storage elements for configurable logic. In 2010 International Conference on Field-Programmable Technology (FPT), pages 17–20. IEEE, 2010.
- [10] Yibo Chen, Jishen Zhao, and Yuan Xie. 3d-nonar: three-dimensional non-volatile fpga architecture using phase change memory. In Proceedings of the 16th ACM/IEEE international symposium on Low power electronics and design, pages 55–60. ACM, 2010.
- [11] Albert Lee, Chieh-Pu Lo, Chien-Chen Lin, Wei-Hao Chen, Kuo-Hsiang Hsu, Zhibo Wang, Fang Su, Zhe Yuan, Qi Wei, Ya-Chin King, and Chrong-Jung Lin. A rram-based nonvolatile flip-flop with self-write-termination scheme for frequent-off fast-wake-up nonvolatile processors. IEEE Journal of Solid-State Circuits, 52(8):2194–2207, 2017.
- [12] Vilabha S Patil, Yashwant B Mane, and Shraddha Deshpande. Fpga based power saving technique for sensor node in wireless sensor network (wsn). In Computational Intelligence in Sensor Networks, pages 385–404. Springer, 2019.
- [13] Billel Bengherbia, Mohamed Ould Zmirli, Abdelmoghni Toubal, and Abderrezak Guessoum. Fpga-based wireless sensor nodes for vibration monitoring system and fault diagnosis. Measurement, 101:81–92, 2017.
- [14] Abdulfattah M Obeid, Fatma Karray, Mohamed Wassim Jmal, Mohamed Abid, Syed Manzoor Qasim, and Mohammed S BenSaleh. Towards realisation of wireless sensor network-based water pipeline monitoring systems: a comprehensive review of techniques and platforms. IET science, measurement & technology, 10(5):420–426, 2016.
- [15] T Xue and S Roundy. Analysis of magnetic plucking configurations for frequency up-converting harvesters. In Journal of Physics: Conference Series, volume 660, page 012098. IOP Publishing, 2015.
- [16] Kaisheng Ma, Xueqing Li, Jinyang Li, Yongpan Liu, Yuan Xie, Jack Sampson, Mahmut Taylan Kandemir, and Vijaykrishnan Narayanan. Incidental computing on iot nonvolatile processors. In Proceedings of the 50th Annual IEEE/ACM International Symposium on Microarchitecture, pages 204–218. ACM, 2017.
- [17] Kaisheng Ma, Xueqing Li, Shuangchen Li, Yongpan Liu, John Jack Sampson, Yuan Xie, and Vijaykrishnan Narayanan. Nonvolatile processor architecture exploration for energy-harvesting applications. IEEE Micro, 35(5):32–40, 2015.
- [18] Kiwan Maeng, Alexei Colin, and Brandon Lucia. Alpaca: intermittent execution without checkpoints. Proceedings of the ACM on Programming Languages, 1(OOPSLA):96, 2017.
- [19] Chen Pan, Mimi Xie, Yongpan Liu, Yanzhi Wang, Chun Jason Xue, Yuangang Wang, Yiran Chen, and Jingtong Hu. A lightweight progress maximization scheduler for non-volatile processor under unstable energy harvesting. In Proceedings of the 18th ACM SIGPLAN/SIGBED Conference on Languages, Compilers, and Tools for Embedded Systems, pages 101–110. ACM, 2017.
- [20] Domenico Balsamo, Alex S Weddell, Geoff V Merrett, Bashir M Al-Hashimi, Davide Brunelli, and Luca Benini. Hibernus: Sustaining computation during intermittent supply for energy-harvesting systems. IEEE Embedded Systems Letters, 7(1):15–18, 2015.
- [21] Mimi Xie, Mengying Zhao, Chen Pan, Jingtong Hu, Yongpan Liu, and Chun Jason Xue. Fixing the broken time machine: Consistency-aware checkpointing for energy harvesting powered non-volatile processor. In Proceedings of the 52nd Annual Design Automation Conference, page 184. ACM, 2015.
- [22] Mimi Xie, Mengying Zhao, Chen Pan, Hehe Li, Yongpan Liu, Youtao Zhang, Chun Jason Xue, and Jingtong Hu. Checkpoint aware hybrid cache architecture for nv processor in energy harvesting powered systems. In Proceedings of the Eleventh IEEE/ACM/IFIP International Conference on Hardware/Software Codesign and System Synthesis, page 22. ACM, 2016.
- [23] Azalia Mirhoseini, Bitar Darvish Rouhani, Ebrahim Songhori, and Farinaz Koushanfar. Chime: Checkpointing long computations on intermittently energized iot devices. IEEE Transactions on Multi-Scale Computing Systems, 2(4):277–290, 2016.
- [24] Zhe Yuan, Yongpan Liu, Hehe Li, and Huazhong Yang. Cp-fpga: Computation data-aware software/hardware co-design for nonvolatile fpgas based on checkpointing techniques. In Design Automation Conference (ASP-DAC), 2016 21st Asia and South Pacific, pages 569–574. IEEE, 2016.
- [25] P-E Gaillardon, Davide Sacchetto, Giovanni Betti Beneventi, M Haykel Ben Jamaa, Luca Perniola, Fabien Clermidy, Ian O’Connor, and Giovanni De Micheli. Design and architectural assessment of 3-d resistive memory technologies in fpgas. IEEE Transactions on Nanotechnology, 12(1):40–50, 2013.
- [26] Jason Cong and Bingjun Xiao. mrfpga: A novel fpga architecture with memristor-based reconfiguration. In 2011 IEEE/ACM International Symposium on Nanoscale Architectures, pages 1–8. IEEE, 2011.
- [27] Ramtin Zand and Ronald F DeMara. Radiation-hardened mram-based lut for non-volatile fpga soft error mitigation with multi-node upset tolerance. Journal of Physics D: Applied Physics, 50(50):505002, 2017.

- [28] Kangwook Jo, Kyungseon Cho, and Hongil Yoon. Variation-tolerant and low power look-up table (lut) using spin-torque transfer magnetic ram for non-volatile field programmable gate array (fpga). In 2016 International SoC Design Conference (ISOCC), pages 101–102. IEEE, 2016.
- [29] Haider Abbas F Almurib, Thulasiraman Nandha Kumar, and Fabrizio Lombardi. Design and evaluation of a memristor-based look-up table for non-volatile field programmable gate arrays. IET Circuits, Devices & Systems, 10(4):292–300, 2016.
- [30] Ramin Rajaei. Radiation-hardened design of nonvolatile mram-based fpga. IEEE Transactions on Magnetics, 52(10):1–10, 2016.
- [31] Lei Ju, Xiaojin Sui, Shiqing Li, Mengying Zhao, Chun Jason Xue, Jingtong Hu, and Zhiping Jia. Nvm-based fpga block ram with adaptive slc-mlc conversion. IEEE Transactions on Computer-Aided Design of Integrated Circuits and Systems, 37(11):2661–2672, 2018.
- [32] H-S Philip Wong, Heng-Yuan Lee, Shimeng Yu, Yu-Sheng Chen, Yi Wu, Pang-Shiu Chen, Byoungil Lee, Frederick T Chen, and Ming-Jinn Tsai. Metal-oxide rram. Proceedings of the IEEE, 100(6):1951–1970, 2012.
- [33] Santhosh Onkaraiyah, Marina Reyboz, Fabien Clermidy, Jean-Michel Portal, Marc Bocquet, Christophe Muller, Hraziaia, Costin Anghel, and Amara Amara. Bipolar rram based non-volatile flip-flops for low-power architectures. In 2012 IEEE 10th International New Circuits and Systems Conference (NEWCAS), pages 417–420. IEEE, 2012.
- [34] K Jabeur, G Di Pendina, and G Prenat. Ultra-energy-efficient cmos/magnetic nonvolatile flip-flop based on spin-orbit torque device. Electronics Letters, 50(8):585–587, 2014.
- [35] Tsai-Kan Chien, Lih-Yih Chiou, Yao-Chun Chuang, Shyh-Shyuan Sheu, Heng-Yuan Li, Pei-Hua Wang, Tzu-Kun Ku, Ming-Jinn Tsai, and Chih-I Wu Wu. A low store energy and robust rram-based flip-flop for normally off microprocessors. In 2016 IEEE International Symposium on Circuits and Systems (ISCAS), pages 2803–2806. IEEE, 2016.
- [36] Xilinx. Xilinx floorplanning methodology guide. Xilinx, 2009.
- [37] Razvan Nane, Vlad-Mihai Sima, Christian Pilato, Jongsok Choi, Blair Fort, Andrew Canis, Yu Ting Chen, Hsuan Hsiao, Stephen Brown, Fabrizio Ferrandi, et al. A survey and evaluation of fpga high-level synthesis tools. IEEE Transactions on Computer-Aided Design of Integrated Circuits and Systems, 35(10):1591–1604, 2015.
- [38] Denis Navarro, Óscar Luci, Luis A Barragán, Isidro Urriza, Oscar Jimenez, et al. High-level synthesis for accelerating the fpga implementation of computationally demanding control algorithms for power converters. IEEE Transactions on Industrial Informatics, 9(3):1371–1379, 2013.
- [39] Weiwen Jiang, Edwin H-M Sha, Xinyi Zhang, Lei Yang, Qingfeng Zhuge, Yiyu Shi, and Jingtong Hu. Achieving super-linear speedup across multi-fpga for real-time dnn inference. ACM Transactions on Embedded Computing Systems (TECS), 18(5s):67, 2019.
- [40] Weiwen Jiang, Xinyi Zhang, Edwin H-M Sha, Lei Yang, Qingfeng Zhuge, Yiyu Shi, and Jingtong Hu. Accuracy vs. efficiency: Achieving both through fpga-implementation aware neural architecture search. arXiv preprint arXiv:1901.11211, 2019.
- [41] Andrew Canis, Jongsok Choi, Mark Aldham, Victor Zhang, Ahmed Kammoona, Tomasz Czajkowski, Stephen D Brown, and Jason H Anderson. Legup: An open-source high-level synthesis tool for fpga-based processor/accelerator systems. ACM Transactions on Embedded Computing Systems (TECS), 13(2):24, 2013.
- [42] Saad Ahmed, Muhammad Hamad Alizai, Junaid Haroon Siddiqui, Naveed Anwar Bhatti, and Luca Mottola. Towards smaller checkpoints for better intermittent computing. In 2018 17th ACM/IEEE International Conference on Information Processing in Sensor Networks (IPSN), pages 132–133. IEEE, 2018.
- [43] Xinyi Zhang, Clay Patterson, Yongpan Liu, Chengmo Yang, Chun Jason Xue, and Jingtong Hu. Low overhead online checkpoint for intermittently powered non-volatile fpgas. In 2018 IEEE Computer Society Annual Symposium on VLSI (ISVLSI), pages 238–244. IEEE, 2018.
- [44] Masood Qazi, Amerasekera Ajith, and Anantha P. Chandrakasan. A 3.4pj feram-enabled d flip-flop in 0.13m cmos for nonvolatile processing in digital systems. In 2013 IEEE International Solid-State Circuits Conference Digest of Technical Papers. IEEE, 2013.
- [45] Farheen Fatima Khan and Andy Ye. A study on the accuracy of minimum width transistor area in estimating fpga layout area. Microprocessors and Microsystems, 52:287–298, 2017.
- [46] Srihari Cadambi, Abhinandan Majumdar, Michela Becchi, Srimat Chakradhar, and Hans Peter Graf. A programmable parallel accelerator for learning and classification. In Proceedings of the 19th international conference on Parallel architectures and compilation techniques, pages 273–284. ACM, 2010.
- [47] Srimat Chakradhar, Murugan Sankaradas, Venkata Jakkula, and Srihari Cadambi. A dynamically configurable coprocessor for convolutional neural networks. ACM SIGARCH Computer Architecture News, 38(3):247–257, 2010.
- [48] Yuko Hara, Hiroyuki Tomiyama, Shinya Honda, and Hiroaki Takada. Proposal and quantitative analysis of the chstone benchmark program suite for practical c-based high-level synthesis. Journal of Information Processing, 17:242–254, 2009.